Electronic Supplementary Material (ESI) for ChemComm.

A new class of electrocatalyst of supporting Pt on an Engel-Brewer alloy substrate: A demonstration for oxidation of ethylene glycol

[1]Xiaofang Yang, [1]Wenqian Xu, [1]Meng Li, [2]Bruce E. Koel* and [3]Jingguang, G. Chen*

[1]Department of Chemistry, Brookhaven National Laboratory, Upton, New York 11973
[2]Department of Chemical and Biological Engineering, Princeton University, Princeton, NJ 08544
[3]Department of Chemical Engineering, Columbia University, New York, NY 10027

1. EXPERIMENTAL AND MODELING METHODS

1.1 Surface Preparation and Characterization in UHV. Three polycrystalline electrodes, ie., Pt, Ir and $HfIr_3$, were polished to a mirror finish and then loaded into a UHV chamber with a base pressure of 2.0×10^{-10} torr. Instrumentation in this chamber included low energy ion scattering (LEIS), Auger electron spectroscopy (AES), and X-ray photoelectron spectroscopy (XPS). The samples were cleaned by cycles of Ar^+ ion sputtering at 1 keV followed by high temperature annealing at 1200 K in vacuum. The Pt monolayer was formed on the cleaned Ir and Hf-Ir surfaces by physical vapor deposition. A Pt doser was constructed by winding Pt wire (d = 0.001″, 5 N, EPSI metals) at the tip region of a V-shaped W wire (d = 0.09″, 3N, EPSI metals) that was attached to a copper power feedthrough mounted on a 2.75″ O.D. conflat flange. Pt metal was deposited on the surface by resistively heating the W wire to 1500 K. Monolayer Pt coverage was obtained in 18 min, using a current of 6.0 A with 2-cm distance between the Pt doser and sample. The Pt coverage was measured by XPS. XPS analysis used Al Kα irradiation and PHI SCA analyzer using 46.7 eV pass energy and take off energy of 70º. Binding energies are referred to $Ir4f_{7/2}$ at 61.3 eV BE. LEIS were done using 3.0 keV Ar^+ ion at 8 nA. The sensitivity factor of Hf:Ir in LEIS is 1.7:1. STM measurements were conducted in a commercial Omicron variable temperature STM system. A tungsten tip (0.010 inches) was chemically etched before used for imaging the surface. Typical imaging conditions are 0.2 nA, 0.5 V. XRD of Hf-Ir alloy was measured at glancing-incidence X-ray beam, 0.3196 Å. The UHV-prepared surfaces could be transferred to an electrochemical cell for electrochemical measurements as described below. As a comparison, a monolayer of Pt was also deposited on a clean polycrystalline Ir sample and a clean polycrystalline Pt sample was prepared in UHV by Ar^+ sputtering and vacuum annealing.

1.2 Electrochemical Measurements. The UHV sample holder could be directly attached to a rotating disc electrode rotator (RDE, Pine). A quick transfer of the sample between the main UHV chamber and the electrochemical cell was accomplished with the aid of a small antechamber/load lock attached to the UHV chamber. Prior to and during the sample transfer, the antechamber was filled with high purity N_2. The UHV-prepared surfaces were protected by a droplet of pure water (HPLC grade, Fisher) and immediately transferred into an electrochemical cell. The sample was immersed in 0.1 M KOH solution for electrochemical measurements by using a hanging-meniscus rotating-disc technique. The height of the meniscus was carefully controlled to prevent the side of the samples from wetting. A standard three-electrode electrochemical cell was used with a Pt-wire counter electrode and a hydrogen electrode as the

reference electrode. More details of sample transfer between UHV and electrochemical cell can be found in our previous paper.[1]

1.3 *In situ* IRRAS Analysis. *In-situ* IRRAS studies were carried out with a Nicolet Nexus 670 Fourier-transform infrared (FTIR) spectrometer equipped with a mercury cadmium telluride (MCT) detector cooled with liquid nitrogen. An unpolarized light beam was used. The spectral resolution was set to 8 cm^{-1} and 128 interferograms were together added to each spectrum. Spectra are given in absorbance units defined as $A = -\log(R/R_0)$, where R and R_0 represent the reflected IR intensities corresponding to the sample- and reference single beam spectrum, respectively. A ZnSe hemisphere was used as the IR window, and the working electrodes used in this IR study, including bulk Pt, Pt-ML/Ir and Pt-ML/Hf-Ir, were pressed against the IR window to create a thin electrolyte layer with a thickness of a few micrometers. Dry air was used to purge the spectrometer and experimental chamber, to remove the spectral interference from CO_2 and water vapor present in beam path. Reference spectra were collected at 50 mV vs. RHE in the same solution with 0.2 mol/L ethylene glycol and 0.1 mol/L KOH, and sample spectra were collected at increasingly higher potentials.

2. Determination of the Pt ML by XPS

Quantification of the Pt coverage on an Ir substrate was based on XPS measurements. Assuming a layer by layer growth mode, the photoelectron intensity from a Pt overlayer, I_{Pt}, raises with thickness of d as: [5]

$$I_{Pt} = I_{Pt}^{\infty}\{1 - \exp\left(-\frac{d}{\lambda_{imfp}^{Pt}(E_{Pt})cos\theta}\right)\} \quad (1)$$

where I_{Pt}^{∞} is the intensity from pure bulk Pt, λ_{impf}^{Pt} is the electron inelastic mean free path (IMFP) of electrons in Pt , at kinetic energy of E_{Pt}, and θ is the emission angle, the angle between the sample normal and detector.

The photoelectron intensity from a Pt overlayer with less than 1 ML can be written as:

$$I_{Pt,\,\alpha_0} = \alpha_0 I_{Pt}^{\infty}\{1 - exp\left(-\frac{d_0}{\lambda_{imfp}^{Pt}(E_{Pt})cos\theta}\right)\}_{=\alpha_0} I_{Pt,\,d_0}\,, \quad (2)$$

where α_0 ($0 < \alpha_0 < 1$) is the Pt coverage and d_0 is thickness of the Pt monolayer, and $I_{Pt,\,d_0}$ is the photoelectron intensity from 1-ML Pt. The Pt intensity linearly increases with coverage in the monolayer and has a slope of $I_{Pt,\,d_0}$.

For an ideal layer-by-layer growth mode, the second Pt layer starts to form after the Ir substrate surface is covered perfectly by the first Pt monolayer. The photoelectron intensity of the thicker Pt overlayer can be written as:

$$I_{Pt,\ \alpha_1} = \alpha_1 I_{Pt}^{\infty}\left\{1 - exp\left(-\frac{d_1}{\lambda_{imfp}^{Pt}(E_{Pt})cos\theta}\right)\right\} + (1-\alpha_1)I_{Pt}^{\infty}\{1 - exp\left(-\frac{d_0}{\lambda_{imfp}^{Pt}(E_{Pt})cos\theta}\right)\} \quad (3)$$

$$= \alpha_1 I_{Pt,\ d_1} + (1-\alpha_1)I_{Pt,\ d_0},$$

$$= \alpha_1(I_{Pt,\ d_1} - I_{Pt,\ d_0}) + I_{Pt,\ d_0}$$, where α_1 ($0< \alpha_1 <1$) is the Pt coverage in the second layer, and d_1 is the thickness of two Pt layers, and $I_{Pt,\ d_1}$ is the photoelectron intensity from two layers of Pt.

The Pt intensity still linearly increases with α_1 and has a slope of $(I_{Pt,\ d_1} - I_{Pt,\ d_0})$. Therefore, the slope of increasing the concentration of Pt in the Pt layer is different from the slope of growing the second Pt layer. Experimentally, one finds a slope-break in the slope of the uptake curves at one Pt monolayer coverage. We monitored the growth of the Pt overlayer on the Ir substrate by recording the Pt 4f and Ir 4f peaks in XPS. Figure S1-a is the raw XPS spectra obtained on Ir after different amounts of Pt dosing. Figure S1-b is the plot of Pt intensity (peak area) versus the dosing time. One can identify a break at 18 min, indicating one monolayer Pt was added on Ir after 18 min. The Pt4f/Ir4f peak ratio is 0.18 and is consistent with the value calculated by Eq. (4):[2]

$$\frac{I_{Pt}/s_{Pt}}{I_{Ir}/s_{Ir}} = \{1 - exp\left(-\frac{d_0}{\lambda_{imfp}^{Pt}(E_{Pt})cos\theta}\right)\} \Big/ exp\left(-\frac{d_0}{\lambda_{imfp}^{Ir}(E_{Ir})cos\theta}\right), \quad (4)$$

where S_{Pt} and S_{Ir} are the sensitivity factors for these Pt and Ir peaks.

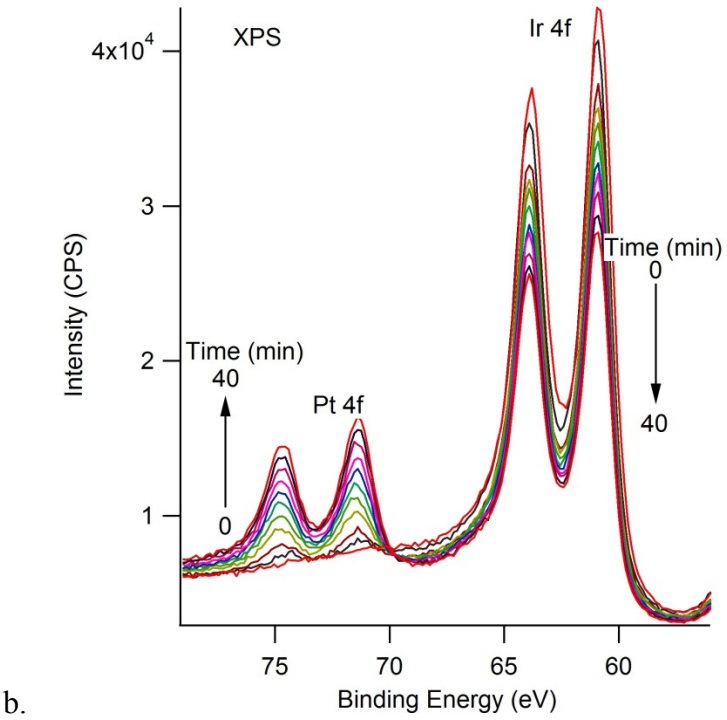

b.

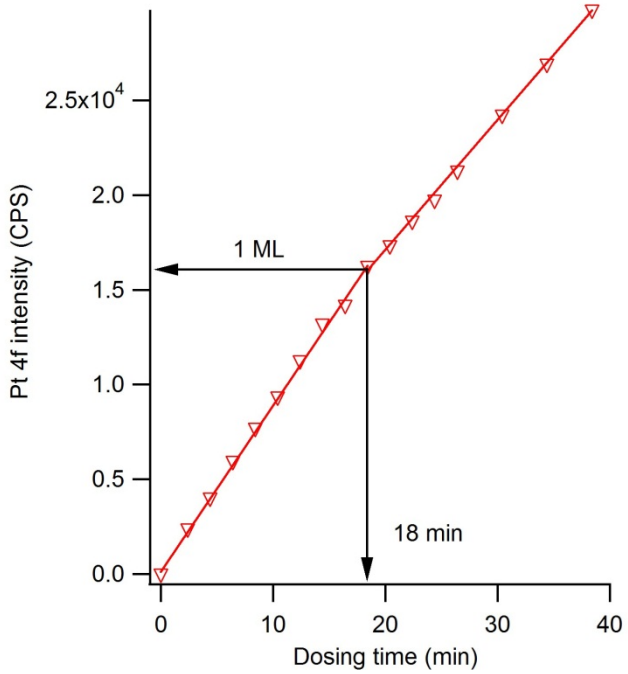

Figure S1. (a) XPS spectra of the Pt 4f and Ir 4f regions for increasing Pt coverage on a Ir polycrystalline substrate. (b). Plot of the Pt 4f intensity versus the dosing time. Arrows mark the break in the uptake curve at 1 ML Pt coverage after 18 min.

3. Cyclic voltammetry of Pt, Pt-ML/Ir and Pt-ML/Hf-Ir in 0.1 M KOH

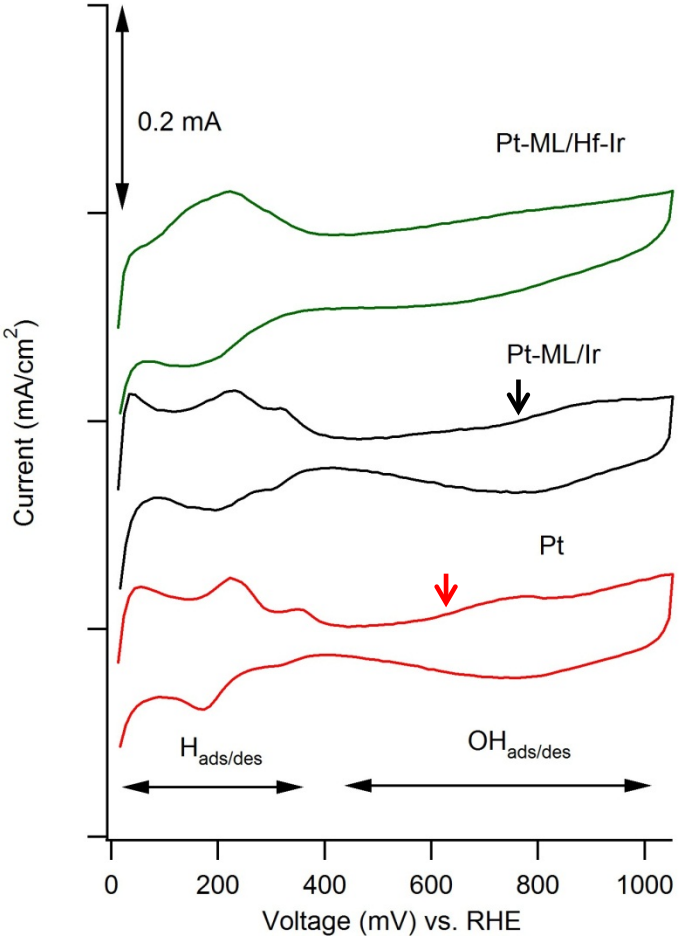

Figure S2. Cyclic voltammetry for Pt, Pt- ML/Ir and Pt-ML/Hf-Ir surfaces in an Ar-purged 0.1 M KOH solution. The sweep rate was 50 mV/s. Arrows indicate the onset of surface oxidation.

The CVs for bulk Pt, Pt-ML/Ir and Pt-ML/Hf-Ir sample are compared in Figure S2. The CV for Pt-ML/Ir was very similar to that for the bulk Pt surface, with the $H_{ads/des}$ regions appearing at below 400 mV, except that the onset potential for surface oxidation on the Pt-ML/Ir surface developed at higher potential than that on the Pt surface. Pt-ML/Hf-Ir exhibits a very different CV. No apparent peak for HO adsorption on Pt-ML/Hf-Ir was found, but this might be because oxidation extends over a wider potential range. The electrochemical surface area can be calculated on the H_{upd} peaks. Assuming the value of 210 μC/cm^2 and a constant double layer current for all of the surfaces, the electrochemical surface areas for Pt, Pt-ML/Ir and Pt-ML/Hf-Ir surfaces are found to be 1.03, 0.94 and 0.95 cm^2 per cm^2 geometric area.

4. Formation of carbonate during EG oxidation

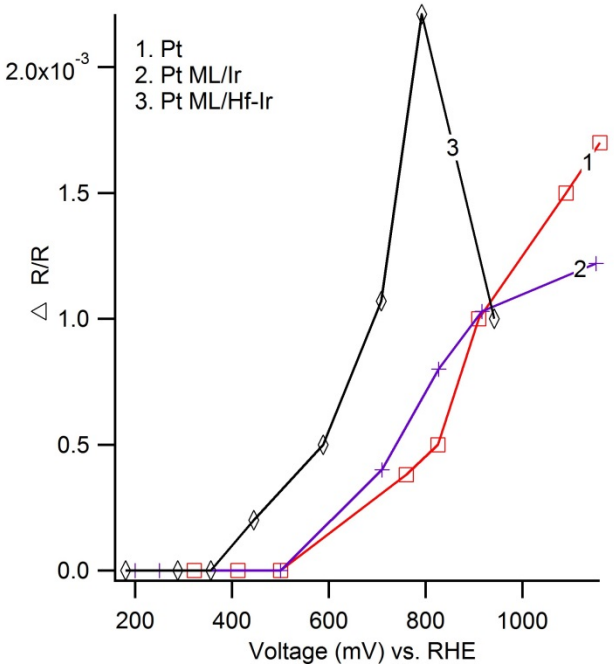

Figure S3. Formation of carbonate during EG oxidation estimated from the peak intensity at ~1400 cm^{-1}

Figure S3 shows the carbonate formation estimated from the peak intensity at 1400 cm^{-1} as the electrode is linearly scanned from low to high potentials. The Pt and Pt ML/Ir surfaces show similar activity. The Pt ML/Hf-Ir surface exhibits three times higher activity than Pt and Pt ML/Ir and the formation of carbonate starts to occur at much lower potentials. The decrease in the carbonate intensity at 940 mV for Pt ML/Hf-Ir is caused by the conversion of carbonate to CO_2 as the electrolyte becomes acidic. Thus, the IRRAS results clearly show that more carbonate is produced by Pt ML/ Hf-Ir surface than Pt.

5. Difference of two continuous spectra

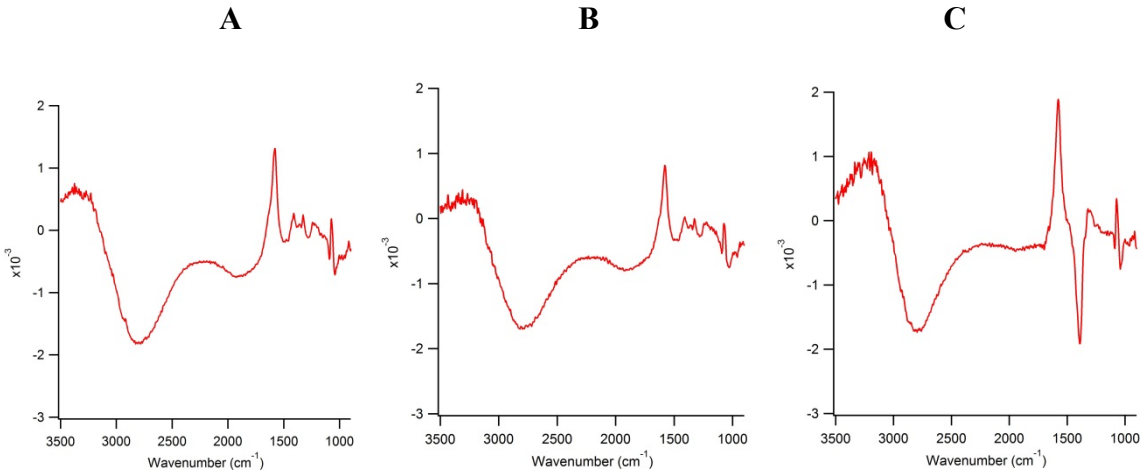

Figure S4. Difference at potentials of 790 and 940 mV. A. Pt, B. Pt ML/Ir and C. Pt ML/Hf-Ir

The difference spectrum is obtained by subtracting the spectrum of 790 mV from that of 940 mV. The difference in two continous IRRAS spectra reflects the quick change of the products during reaction. It can be seen that the difffenece spectra for Pt and Pt/ML are very similar and they appear as the regular spectra at high potentials. However, the difference spectrum for Pt ML/Hf-Ir is different from others. A negative band at 1389 cm^{-1} is caused by the decrease of carbonate concentration as the carbonates transform to CO_2.

6. *In situ* IRAS studies at a fixed potental of 470 mV vs RHE

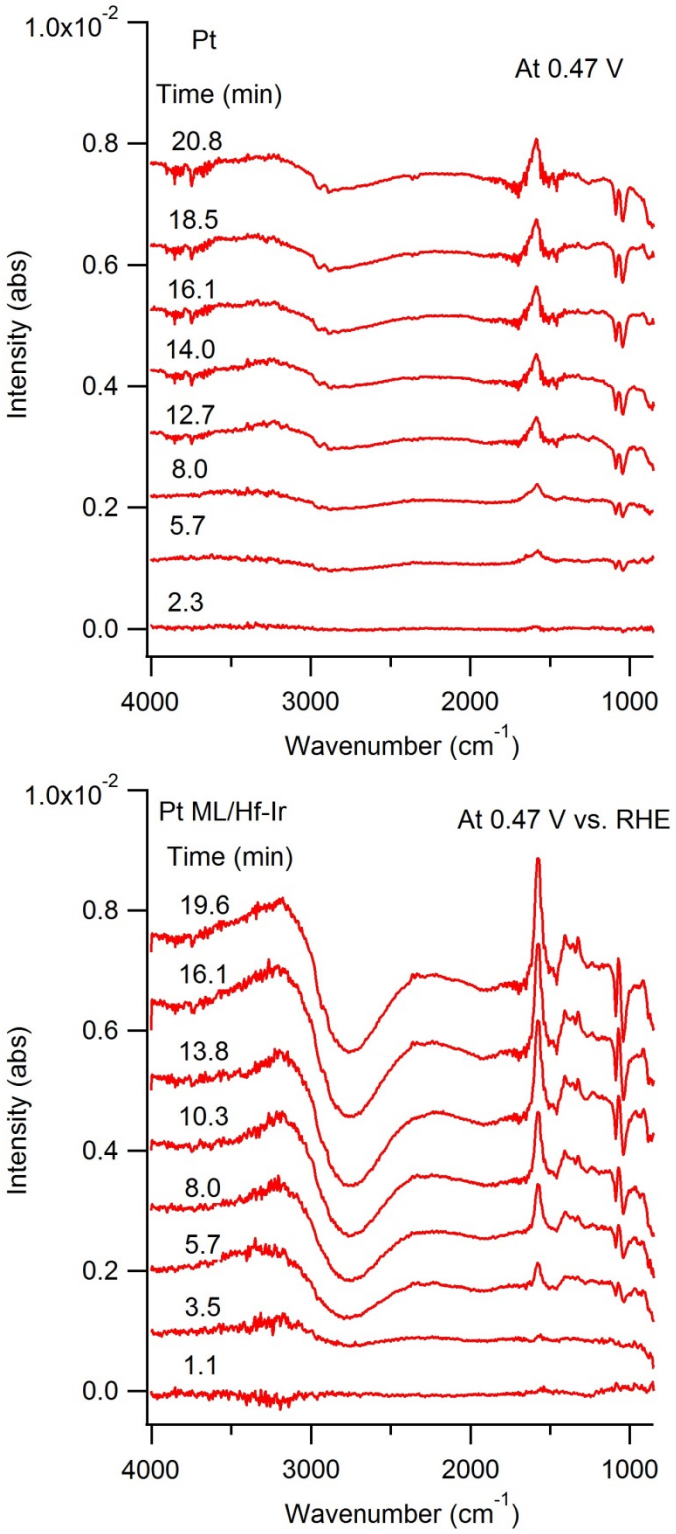

Figure S5. IR spectra of EG oxidation recorded on Pt and Pt ML/Hf-Ir surfaces while maintining the potentia at 470 mV vs. RHE. Carbonates only formed at Pt Ml/Hf-Ir surface at this potential. For IR peak assignment, see main text.

7. Reducibility of Hf oxides on a Hf-Ir alloy

The thermal stability of Hf oxides at the Hf-Ir alloy surface was investigated by annealing Hf-Ir at different temperatures in vacuum after oxidation at 1000 K using 2E-8 torr O_2 for 2 min. The XPS spectra of Hf 4f regions were recorded and compared in Figure S6.

There are three chemical states of Hf peak with Hf $4f_{7/2}$ identified at 14.3 (metal), and 17.9 (HfO_2) eV BE, and suboxides with a broad line shape at intermediate binding energies.[3] We found similar Hf $4f_{7/2}$ peaks at 14.6, and 17.9 eV BE for the Hf-Ir alloy. These were identified as due to metallic Hf alloyed with Ir and fully oxidized HfO_2, respectively. The suboxide component was fitted by a doublet with the Hf $4f_{7/2}$ peak at 16.4 eV BE and the Hf $4f_{5/2}$ at 18.04 eV BE. Annealing the pre-oxidized surface in vacuum at 600 K for 3 min caused a large decrease in the HfO_2 peak. This demonstrates that fully oxided Hf can be relatively easily reduced to some partially oxidized state, HfO_x, by low tempeature annealing in vacuum, which indicates some oxygen atoms are weakly bonded to Hf.

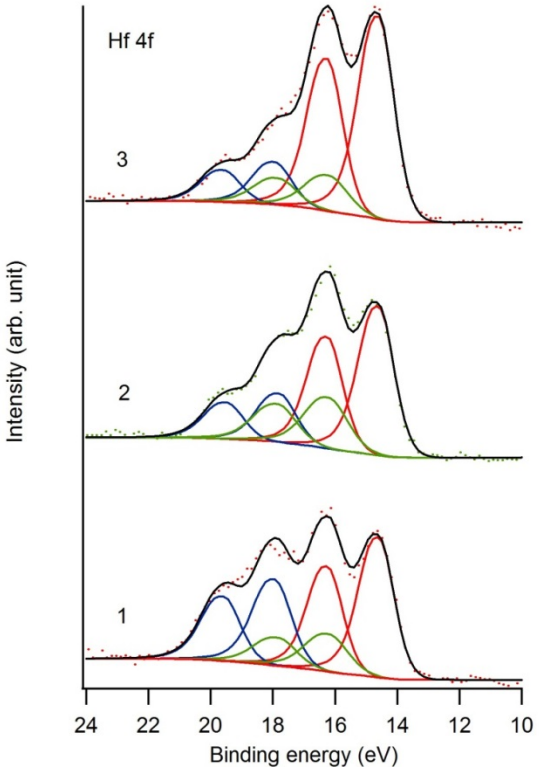

Figure S6. XPS Hf 4f spectra of the Hf-Ir alloy. 1.After oxidation at 600 K with 2.0 $\times 10^{-8}$ torr O_2, 2 min. 2. After (1) and annealing in vacuum at 600 K for 3 min. 3. After (2) and annealing in vacuum at 1000 K for 3 min. The Hf $4f_{7/2}$ peaks at 14.6 eV, 16.3, and 17.9 eV BE are assigned as metallic Hf (red), Hf sub-oxide (green) and HfO_2(blue), respectively. Curves were fitted using a constant spin-orbit splitting of 1.64 eV.

8. Cataltic acitivy of Pt ML/Hf

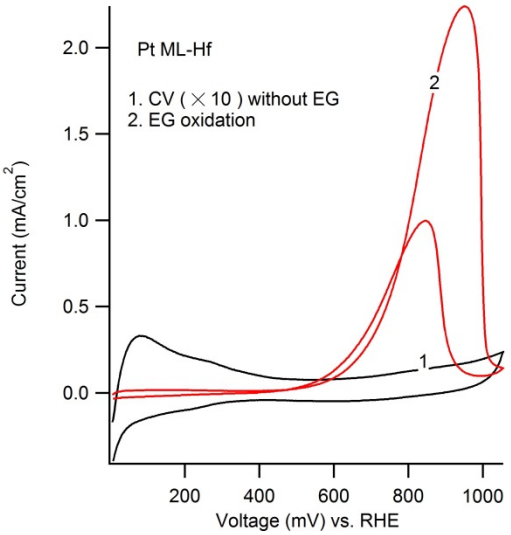

Figure S7. Activity of Pt ML/Hf for EG oxidation. 0.2 mol/L EG in 0.1 mol/L KOH at 25 ºC. Cyclic voltammogram (CV) of 10th scan with a scan rate of 50 mV/s is shown. The activity of Pt ML/Hf for EG oxidation. The activity of the Pt ML/Hf is much lower than Pt ML/Ir and Pt ML/Hf-Ir. It is even lower than pure Pt but it shows a similar feature to the Pt in terms of the development of oxidation peaks. Thus, the formation of Hf oxide alone is not sufficient to improve the performance of the Pt layer. The altered electronic property of the Pt ML by the substrate is the main reason, which could explain the large improvement from Pt to Pt ML/Ir. However, the presence of Hf oxide is also very important to improve the selectivity to CO_2 product. As it is seen in the IRRAS measurements, the main products by Pt ML-Ir are from still incomplete oxidation of EG. When the HfO_x is present, more carbonate /CO_2 is produced. Therefore, the enhanced performance could be associated with both the high reducibility of Hf oxide and altered electronic property of the Pt ML.

Table 1 IRRAS Spectra Band Assignments

Wavenumber / cm^{-1}	Assignment
1577	Unsymmetrical stretching of –C=OO group in glycolate or oxalate [4,5]
1409	Symmetrical stretching of –C=OO group in glycolate or oxalate [5]
1072	-C-OH stretching in glycolate [5]
1231	C-O stretching in glycolate [5]
1357	Adsorbed carboxylate [4]
1322	C-O stretching in oxalate [5]
~1400	Carbonate [4]
2340	CO_2 in solution [4]
2500-3000	OH^- [4]

References

(1) X. Yang, Y.C. Kimmel, J. Fu, B. E. Koel, and J.G. Chen, ACS Catalysis 2012, 2, 765–769.
(2) Cumpson, P. J.; Seah, M. P. Surface and Interface Analysis 1997, 25, 430.
(3) Morant, C.; Galán, L.; Sanz, J. M. Surface and Interface Analysis 1990, 16, 304.
(4)Christensen, P. A.; Hamnett, A. J. Electroanal. Chem. Interfacial Electrochem. 1989, 260, 347.
(5) Max, J.-J.; Chapados, C. The Journal of Physical Chemistry A 2004, 108, 3324.